Available online at www.sciencedirect.com

SciVerse ScienceDirect

Ceramics International 39 (2013) 5077–5082

CERAMICS INTERNATIONAL

www.elsevier.com/locate/ceramint

Spark plasma sintering of TiC-based composites toughened by submicron SiC particles

Lixia Cheng[a], Zhipeng Xie[a,*], Guanwei Liu[b]

[a]State Key Laboratory of New Ceramics and Fine Processing, Department of Materials Science and Engineering, Tsinghua University, Beijing 100084, PR China

[b]R&D Center for Vehicle Battery and Energy Storage, General Research Institute for Nonferrous Metals, Beijing, 100088, PR China

Received 26 October 2012; received in revised form 1 December 2012; accepted 1 December 2012
Available online 10 December 2012

Abstract

TiC-based composites toughened by submicron SiC particles with improved fracture toughness were fabricated and fracture mechanism has been investigated. It has been found that the improvement in fracture toughness of TiC–SiC composites is due to both crack paths propagating through uniformly distributed SiC particles and the fracture mode transition from intergranular type to transgranular type caused by the change of residual stresses originating from the addition of SiC particles. The optimum of fracture toughness (5.2 MPa $m^{1/2}$) was achieved at 14.6 vol% SiC, whereas the toughness decreased with increasing amount of SiC beyond 30 vol%.

Keywords: TiC–SiC; Fracture toughness; Fracture mechanism; Spark plasma sintering

1. Introduction

Titanium carbide (TiC) ceramics with covalent bonding possess high melting temperature (~3260 °C), high electrical conductivity ($30 \times 10^6/\Omega$ cm), high chemical and thermal stability, good corrosion resistance [1] and high hardness (~30.3 GPa) [2]. Because of this combination of properties, TiC ceramics have been widely applied in cutting tools and machining materials. Additional interest in TiC has been generated due to recent research activity related to nuclear industry in recent years. Benefiting from the low neutron absorption cross-section, TiC has been proposed as one of the inert matrix fuels (IMF) or diluting agents for fast reactors [3,4]. However, the modest fracture toughness of TiC ceramics limits their use under severe conditions. It is, therefore, highly desirable to improve the fracture toughness of TiC.

Previous investigations have shown that the dispersion of second-phase particles into ceramic matrix can improve their mechanical properties, e.g., TiC particles in Al_2O_3 matrix [5], WC particles in ZrB_2–SiC matrix [6], TiB_2 particles in B_4C [7] and SiC particulates reinforced mullite composites foams [8]. Due to relatively good mechanical properties and excellent oxidation resistance [9], the addition of SiC particles, therefore, can not only enhance the mechanical properties of TiC ceramics but also improve their oxidation resistance as well. Titanium carbide ceramics reinforced by SiC particles have been investigated in recent years; however, most of the investigations were concerning on the effects of nano-SiC particles on the mechanical properties of TiC ceramics [10,11]. Furthermore, the cost of nano-powders is relatively high and the dispersion of nano-powders is more difficult, and thus it is necessary to develop high performance TiC-based composites by adding submicron SiC particles. Chen et al. [9] fabricated TiC–SiC composites with improved hardness by adding certain amount of submicron SiC particles, but fracture toughness was not tested in their experiment. In addition, there are few reports discussing the toughening mechanism of SiC particles in TiC-based composites up to now.

*Corresponding author. Tel.: +86 10 6279 9031; fax: +86 10 6277 1161.
E-mail address: xzp@mail.tsinghua.edu.cn (Z. Xie).

0272-8842/$ - see front matter © 2013 Published by Elsevier Ltd and Techna Group S.r.l.
http://dx.doi.org/10.1016/j.ceramint.2012.12.002

In the present work TiC-based composites with different contents of submicron SiC particles were fabricated by spark plasma sintering (SPS) at 1600 °C for 5 min, and the microstructure–fracture toughness relationship of obtained ceramics was investigated. Additionally, theoretical calculations and analysis were used to further study the fracture mechanism.

2. Experimental procedures

Commercially available TiC (~2 μm particle size, ST-Nano Science & Technology Co., Ltd., Shanghai, China) and SiC powders (average particle size ~300 nm, Weifang Kaihua silicon carbide powder Co., Ltd., Weifang, China) were used as raw materials. In order to get uniform powder mixtures with different amounts of SiC additions (14.6, 27.7, 39.7 and 50.6 vol%, which denoted as TS-1, TS-2, TS-3 and TS-4, respectively.), two-step method was used. Firstly, TiC and SiC powders were ultrasonically treated in absolute ethanol for 20 min. After that, the suspension mixtures containing TiC and SiC were further blended by ultrasonic treatment for another 20 min. Secondly, the TiC–SiC suspension mixtures were poured into a polyurethane jar and ball milled for 6 h at 300 rpm using silicon carbide milling media. The mixtures were subsequently dried in a rotary evaporator at 70 °C and then the dried powder mixtures were crashed and sieved to −80 mesh screen size. About 5 g of powders was filled into a graphite die with an inside diameter of 20 mm and sintered with a spark plasma sintering (SPS) apparatus (Dr. Sinter SPS-1050T, Sumitomo Coal Mining Co. Ltd., Japan) in vacuum. An infrared thermometer was used to measure the temperature. A schematic drawing of the SPS apparatus used in this investigation is shown in Fig. 1. All the samples were sintered at 1600 °C for 5 min under 50 MPa.

The bulk densities of all sintered pellets were measured using the Archimedes method. Relative density was calculated by the measured bulk density and theoretical density which is calculated according to the mixture rule. The change of crystalline phase compositions of the samples after sintering was identified by X-ray diffraction (XRD) using CuKα radiation (Dmax-2500 diffractometer, Rigaku, Japan). Microstructures were investigated by field-emission scanning electron microscope (FESEM, LEO-1530, Leo, Oberkochen, Germany) using both secondary electron (SE) and backscattered electron (BSE) imaging. The average grain size of the sintered specimens was estimated through at least 120 grains on FESEM micrographs of the polished and etched surface by image analysis techniques. The Vickers hardness (H_V) was measured by the Vickers indentation test (HV-120; Lai Zhou Hardness Tester Manufactory, China), and the applied load and dwell time were 49 N and 10 min, respectively. Fracture toughness (K_{IC}) was calculated according to the equation given by Anstis et al. [12]:

$$K_{IC} = 0.016\left(\frac{E}{H_V}\right)^{1/2}\left(\frac{P}{c}\right)^{3/2} \quad (1)$$

where E is the elastic modulus (Pa) obtained by the ultrasonic velocity measurements, H_V is the Vickers hardness (Pa), P is the applied load (N), and c is the average crack length.

3. Results and discussion

Fig. 2 shows XRD patterns of TiC composites with different contents of SiC after sintering. Only TiC and SiC peaks are observed in the XRD patterns, indicating that no obvious reaction of TiC and SiC took place in the sintering process. The grain morphology presented in the microstructures was studied using back-scattered electrons in FESEM micrographs of TiC–SiC composites, which are shown in Fig. 3. In case of TiC–SiC composites, two phases with gray and black were observed. The energy-dispersive X-ray spectroscopy (EDS) analysis further confirmed that the gray phase was TiC and the black phase

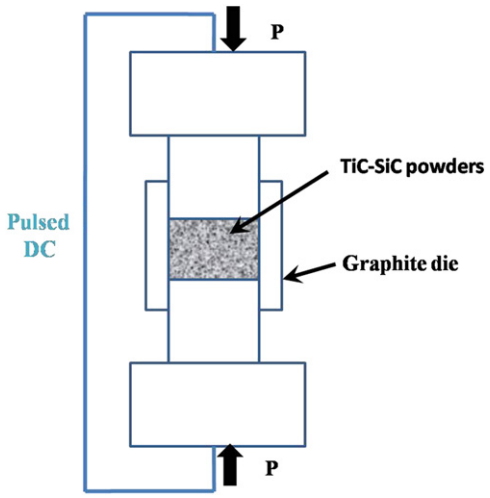

Fig. 1. Schematic drawing of the spark plasma sintering (SPS) apparatus.

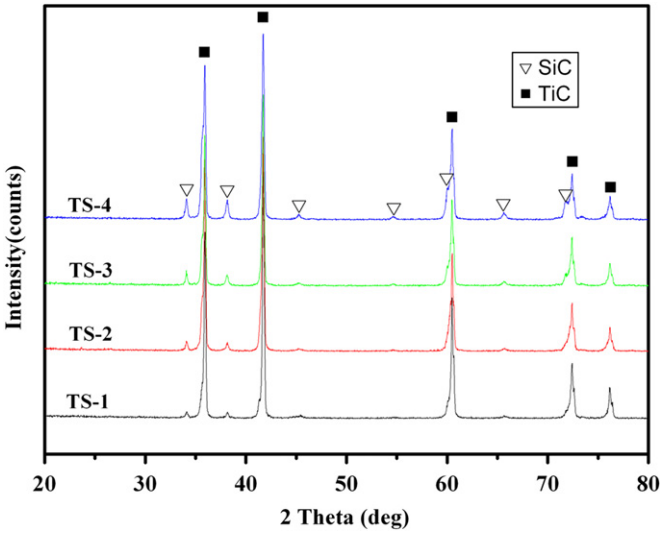

Fig. 2. XRD patterns of TiC–SiC samples.

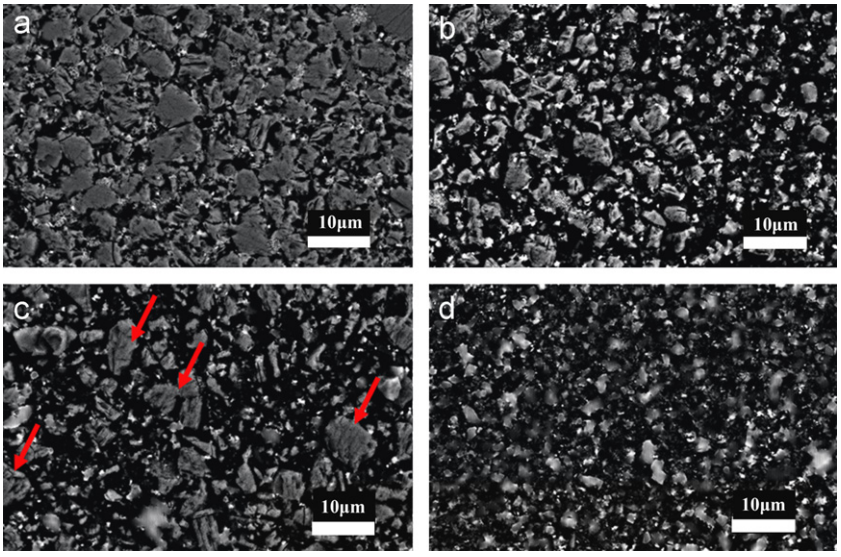

Fig. 3. Back-scattered electron (BSE) images of etched surface of TiC–SiC samples (a) TS-1; (b) TS-2; (c) TS-3; and (d) TS-4.

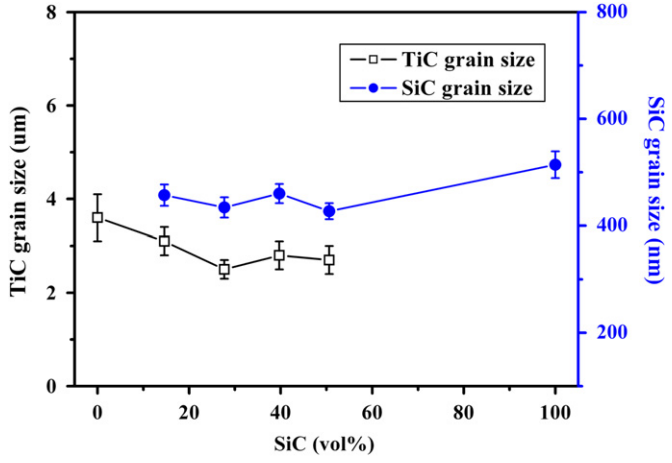

Fig. 4. Average grain size of TiC–SiC composites vs. SiC content.

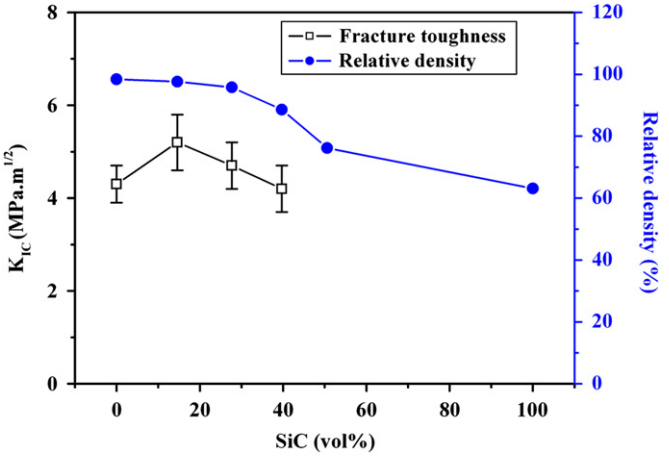

Fig. 5. Fracture toughness and relative density of TiC–SiC composites vs. SiC content.

was SiC. With increasing SiC content, the volume fraction of black parts increased and finer microstructure was obtained. As shown in Fig. 3, the average TiC grain size in TiC–SiC composites decreased with SiC content from ~3.6 μm to ~2.5 μm. It is believed that SiC particles retarded the TiC grain growth by pinning and prohibiting the grain boundary movement. However, compared to the microstructure of the sample TS-2, some larger TiC grains, as indicated by the red arrows in Fig. 3c, were observed in the TS-3 sample. Furthermore, the variations of both TiC and SiC particle size with SiC volume fraction were depicted in Fig. 4. It can be seen that the grain size of both TiC and SiC decreased with SiC volume fraction and the finest microstructure could be achieved at 27.7 vol% SiC. In addition, smaller TiC and SiC grains in the TS-4 sample were thought to be related to poor sinterability of SiC powder, which is also corroborated by the relative density shown in Fig. 5 and the fracture microstructures shown in Fig. 6. Moreover, the elevated porosity was observed in samples with increasing SiC content (Fig. 6), which could restrict the grain boundary migration [13]. Additionally, the average grain sizes of TiC and SiC in TiC–SiC composites were smaller than that of corresponding monolithic TiC and SiC ceramics, revealing that mutual inhibition between TiC and SiC grains occurred during sintering.

Fig. 6 shows the fractured surface of pure TiC and SiC ceramics as well as TiC–SiC composites sintered by SPS at 1600 °C under a pressure of 50 MPa. The images of the microstructure verified that the average grain size decreased with increasing of SiC volume fraction, whereas the porosities increased with increasing of SiC volume fraction. Compared to other samples, a more homogenous and finer microstructure could be observed in the TS-2 sample with 27.7 vol% SiC and the average grain size of

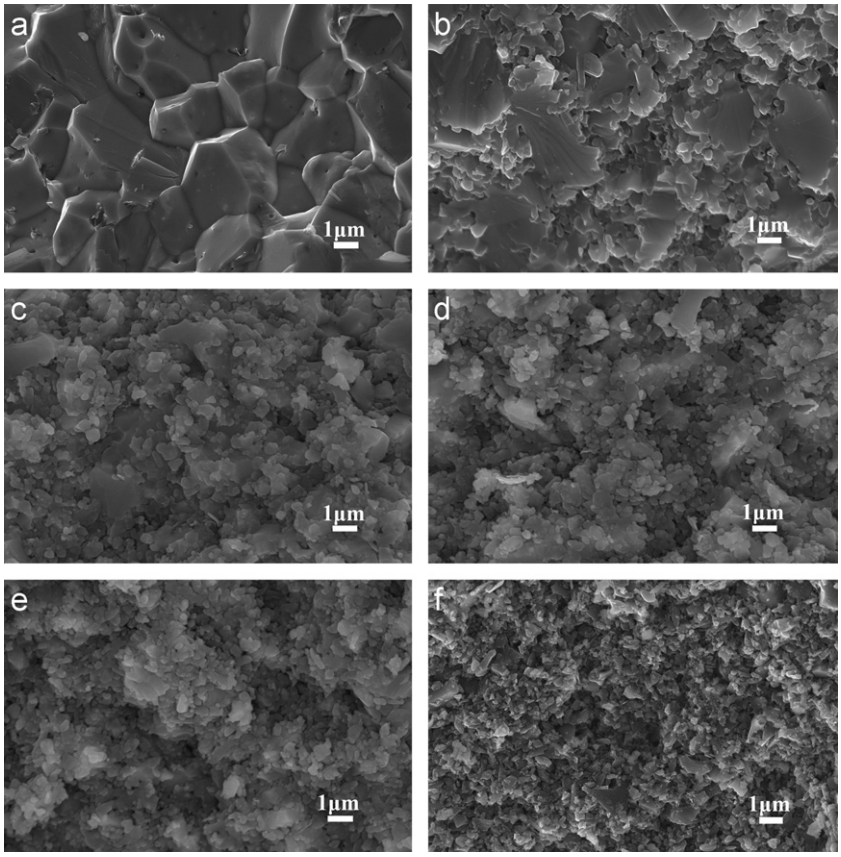

Fig. 6. The fracture micrographs of sample: (a) TiC; (b) TS-1; (c) TS-2; (d) TS-3; (e) TS-4; and (f) SiC.

both TiC and SiC grains were about 2.5 μm and 430 nm, respectively. Although the particle size of TS-1 sample (i.e., TiC—14.6 vol% SiC composite) was slightly larger, the optimum fracture toughness was achieved in this sample due to both higher density and the homogeneous distribution of SiC particles (see Figs. 5 and 6). As can be found in Fig. 5, the fracture toughness of TiC composites with SiC content less than 30 vol% was higher than that of pure TiC and the optimized fracture toughness was realized in the sample with 14.6 vol% SiC additions (5.2 MPa $m^{1/2}$), which was improved by ~21% compared to that of TiC monolithic [2]. The fracture toughness deteriorated continuously with increasing SiC additions, especially when the amount attained a value higher than 30 vol%, and this phenomenon may be attributed to the higher porosity as shown in Figs. 4 and 6. Compared to the results of Ti/submicro-SiC composites investigated by Wang et al. [14], the fracture toughness of TiC—14.6 vol% SiC composites was increased by 44.4%.

As mentioned above, finer microstructure and improvement of fracture toughness were obtained with the addition of submicron SiC particles. To provide evidence of the debonding behavior of ceramic grains and activated toughening mechanisms with adding SiC particles, cracks emerging from Vickers indentations were investigated on the polished and etched surfaces. FESEM images of pure TiC and TiC–SiC composites illustrating typical crack paths are presented in Fig. 7a and b, respectively. It can be seen from Fig. 7a that crack paths on the surface of pure TiC ceramics mainly traveled along grain boundaries (i.e., intergranular fracture mode); however, the crack mostly cleaved SiC grains in the TiC–SiC composite (Fig. 7b) and the fracture mode exhibited a dominating

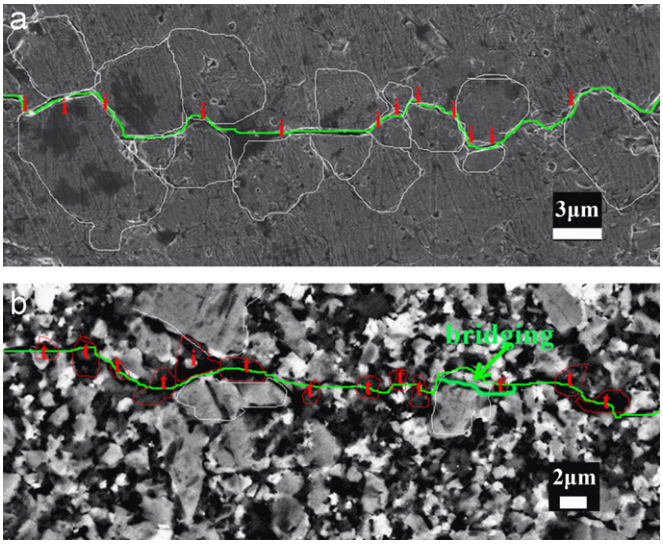

Fig. 7. SEM images of indentation crack propagation of TiC (a) and TS-1(b).

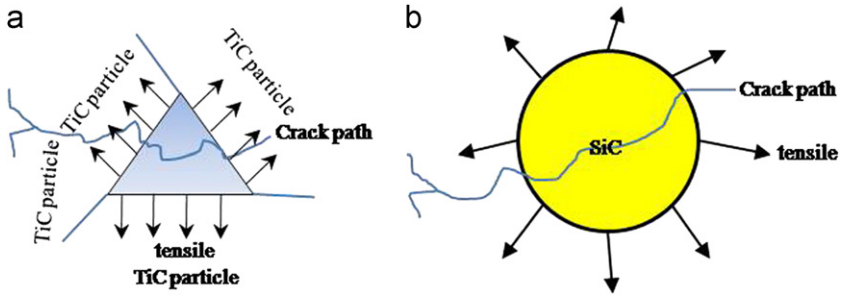

Fig. 8. Schematic illustration of the effect of residual stresses on (a) the fracture mode of grain boundary phases in pure TiC ceramics and (b) SiC particles in TiC–SiC composites.

transgranular type. Furthermore, crack bridging and branching were also observed in the TiC–SiC composite (Fig. 7b).

In order to further elucidate the toughening mechanisms of TiC–SiC composites, a fundamental understanding of improved toughness is provided in the present work. Firstly, for the pure TiC ceramic, the impureoxides (such as TiO_2) existed in the grain boundaries are not unavoidable. So we should consider the residual stresses originating from the thermal expansion mismatch between TiC grains and grain boundary phases. Therefore, a widely used equation is introduced to calculate the residual stresses of pure TiC ceramic according to Peterson and Tien [15],

$$\sigma_m = (\alpha_m - \alpha_g)\left[\frac{1-2v_m}{E_m} + \frac{1+f_m+v_g(1-4f_m)}{2E_g(1-f_m)}\right]^{-1}\Delta T \quad (2)$$

and

$$\sigma_g = -\frac{f_m}{1-f_m}\sigma_{mr} \quad (3)$$

where σ_m and σ_g are the residual stresses in the TiC matrix and grain boundary, respectively; α_m and α_g are the thermal expansion coefficients of TiC and grain boundary phase; ΔT is the difference in temperature over which stresses are not relieved by a diffusion process (assuming 1000 °C); f_m is the volume fraction of the TiC matrix (87.8 vol% from SEM images of the polished and etched surface calculation), v_m (0.27 for matrix phase) and E_m, and v_g (0.27 for grain boundary phase) and E_g are the Poisson ratio and Young modulus of TiC and grain boundary phase, respectively.

Secondly, for the TiC–SiC composite, the mismatch between the linear thermal expansion coefficients (α) and elastic modulus (E) in the TiC matrix and the SiC particle results in the generation of residual stresses in the particles and surrounding matrix during cooling after fabrication. In the present paper, analysis of the residual stresses is based on the hydrostatic stress (σ_h) developed with the particle according to the following equation [16]:

$$\boldsymbol{\sigma}_m = -\frac{(\boldsymbol{\alpha}_m - \boldsymbol{\alpha}_p)\Delta T}{[(1+\boldsymbol{v}_m)/2E_m] + [(1-2\boldsymbol{v}_p)/E_p]} \quad (4)$$

where σ_m, v_m and E_m are the residual stresses, Poisson ratio and Young modulus of TiC, respectively; v_p and E_p are the Poisson's ratio and Young's modulus of SiC particles (assuming $v_m = v_p$ in the present work).

Assigning $7.4\times10^{-6}\,°C^{-1}$, $9.0\times10^{-6}\,°C^{-1}$ and $4.8\times10^{-6}\,°C^{-1}$ to α_m(TiC), α_g(TiO_2) and α_p(SiC), and 447 GPa, 230 GPa and 440 GPa to E_m, E_g and E_p, respectively. Combining Eqs. (2) and (3), we can obtain the stresses in the pure TiC ceramics. The stress on the TiC particle was compressive (−) and that on grain boundary phase was tensile (∼ +500 MPa) in nature. Therefore, it is easy for cracks to propagate through the weaker grain boundary phase (see Fig. 7a), resulting in intergranular fracture behavior [14]. Based on Eq. (4), the stresses in TiC grains of TiC–SiC composites were compressive (−) similar to those in the pure TiC ceramic, while the tensile stresses (∼ +1000 MPa) were calculated in SiC particles, indicating that the crack path would propagate along SiC grains rather than TiC matrix grains and result in transgranular fracture, which is consistent with Fig. 7b.

To understand the fracture mode change caused by the variation of residual stresses more clearly, a schematic illustration of interaction between the propagating crack and the TiC particle in the presence of highly localized tensile stresses at triple junctions or SiC particles is shown in Fig. 8. It can be seen that both grain boundary phases (Fig. 8a) and SiC particles (Fig. 8b) are in tensile stresses and the crack would be attracted to them. As mentioned above, the crack propagating through SiC particles rather than along the grain boundary phases in TiC–SiC composites is the biggest difference of the toughening mechanism between pure TiC and TiC–SiC composites. Therefore, fracture mode transition from intergranular type to transgranular type should be the main reason for the improved toughness of TiC–SiC composites. Additional crack bridging and deflection as depicted in Fig. 7b also play important roles in enhancing the toughness. Therefore, the effect of residual stresses on the fracture toughness of TiC–SiC composites was confirmed by satisfactory agreement between the theoretical thermal calculation and the experimental crack path characteristics experimentally above.

4. Conclusions

In the present work, TiC-based composites toughened by submicron SiC particles with improved fracture

toughness have been fabricated by spark plasma sintering (SPS) at 1600 °C for 5 min under 50 MPa. The fracture mechanism has been also systematically investigated. The fracture toughness increased with SiC content less than 30 vol% and the optimum of fracture toughness (5.2 MPa $m^{1/2}$) was achieved at 14.6 vol% SiC. The fracture toughness deteriorated with increasing the amount of SiC beyond 30 vol% due to the significant decrease of density. The theoretical analysis and experimental results proved that the enhanced fracture toughness of TiC-based composites with SiC content less than 30 vol% is due to fracture mode transition caused by the change of residual stresses originating from the addition of SiC particles. Tensile stresses in SiC particles and compressive stresses in TiC matrix particles were observed in TiC–SiC composites, according to a theoretical calculation of residual stresses originating from the mismatch of linear thermal expansion between the matrix and the second phase. It was demonstrated that cracks propagated through SiC particles easily and transgranular fracture mode was formed.

Acknowledgment

This work was financially supported by the National Natural Science Foundation of China (Grant no. 91026008).

References

[1] R. Koc, J.S. Folmer, Synthesis of submicrometer titanium carbide powders, Journal of the American Ceramic Society 80 (1997) 952–956.
[2] L.X. Cheng, Z.P. Xie, G.W. Liu, W.J. Xue, W. Liu, Densification and mechanical properties of TiC by SPS-effects of holding time, sintering temperature and pressure condition, Journal of the European Ceramic Society 32 (2012) 3399–3406.
[3] K.D. Weaver, T.C. Totemeier, D.E. Clark, E.E. Feldman, E.A. Hoffman, R.B. Vilim, et al., Gen IV Nuclear Energy Systems-Gas-Cooled Fast Reactor (GFR); FY-04 Annual Report, Idaho National Engineering and Environmental Laboratory Bechtel BWXT Idaho, LLC, Report no. INEEL/EXT-04-02361, Contract no. DE-AC07-99ID13727, September, 2004.
[4] R. Fielding, M. Meyer, J.F. Jue, J. Gan, Gas-cooled fast reactor fuel fabrication, Journal of Nuclear Materials 371 (2007) 243–249.
[5] J.H. Gong, Z. Zhao, H.Z. Miao, Z.D. Guan, R-curve behavior of TiC particle reinforced Al_2O_3 composites, Scripta Materialia 43 (2000) 27–31.
[6] J. Zou, G.J. Zhang, C.-F. Hu, T. Nishimura, Y. Sakka, J. Vleugels, O. Van der Biest, Strong ZrB_2–SiC–WC ceramics at 1600 °C, Journal of the American Ceramic Society 95 (2012) 874–878.
[7] M. Mashhadi, E. Taheri-Nassaj, M. Mashhadi, V.M. Sglavo, Pressureless sintering of B_4C–TiB_2 composites with Al additions, Ceramics International 37 (2011) 3229–3235.
[8] S. Akpinar, I.M. Kusoglu, O. Ertugrul, K. Onel, Silicon carbide particle reinforced mullite composite foams, Ceramics International 38 (2012) 6163–6169.
[9] J. Chen, W.J. Li, W. Jiang, Characterization of sintered TiC–SiC composites, Ceramics International 35 (2009) 3125–3129.
[10] L.J. Wang, W. Jiang, L.D. Chen, Fabrication and characterization of nano-SiC particles reinforced TiC/SiC nanocomposites, Materials Letters 58 (2004) 1401–1404.
[11] J. Cabrero, F. Audubert, R. Pailler, Fabrication and characterization of sintered TiC–SiC composites, Journal of the European Ceramic Society 31 (2011) 313–320.
[12] G.R. Anstis, P. Chantikul, B.R. Lawn, D.B. Marshall, A critical evaluation of indentation techniques for measuring fracture toughness: I. Direct crack measurements, Journal of the American Ceramic Society 64 (1981) 533–538.
[13] V. Biasini, S. Guicciardi, A. Bellosi, Silicon nitride–silicon carbide composite materials, Refractory Metals and Hard Materials 11 (1992) 213–221.
[14] L.J. Wang, W. Jiang, L.D. Chen, Effect of starting SiC particle size on in situ fabrication of Ti_5Si_3/TiC composites, Materials Science Engineering A 425 (2006) 219–224.
[15] I.M. Peterson, T.Y. Tien, Effect of the grain boundary thermal expansion coefficient on the fracture toughness in silicon nitride, Journal of the American Ceramic Society 78 (1995) 2345–2352.
[16] G.C. Wei, P.F. Becher, Improvements in mechanical properties in SiC by the addition of TiC particles, Journal of the American Ceramic Society 67 (1984) 571–574.